



HAL
open science

Virgo: an unlikely cluster of galaxies because of its environment

Jenny G. Sorce, Joakim A Rosdahl, Yohan Dubois

► **To cite this version:**

Jenny G. Sorce, Joakim A Rosdahl, Yohan Dubois. Virgo: an unlikely cluster of galaxies because of its environment. Monthly Notices of the Royal Astronomical Society, 2019, 486 (3), pp.3951-3962. 10.1093/mnras/stz1080 . hal-02108584

HAL Id: hal-02108584

<https://hal.science/hal-02108584v1>

Submitted on 5 Jul 2023

HAL is a multi-disciplinary open access archive for the deposit and dissemination of scientific research documents, whether they are published or not. The documents may come from teaching and research institutions in France or abroad, or from public or private research centers.

L'archive ouverte pluridisciplinaire **HAL**, est destinée au dépôt et à la diffusion de documents scientifiques de niveau recherche, publiés ou non, émanant des établissements d'enseignement et de recherche français ou étrangers, des laboratoires publics ou privés.

Virgo: an unlikely cluster of galaxies because of its environment

Jenny G. Sorce,^{1,2★} Jérémy Blaizot¹ and Yohan Dubois³

¹Univ Lyon, Univ Lyon1, Ens de Lyon, CNRS, Centre de Recherche Astrophysique de Lyon UMR5574, F-69230 Saint-Genis-Laval, France

²Leibniz-Institut für Astrophysik, An der Sternwarte 16, D-14482 Potsdam, Germany

³Institut d'Astrophysique de Paris, UMR 7095 CNRS et Université Pierre et Marie Curie, 98bis Bd Arago, F-75014 Paris, France

Accepted 2019 April 11. Received 2019 March 20; in original form 2018 November 8

ABSTRACT

Galaxy clusters constitute powerful cosmological probes thanks to comparisons between observed and simulated clusters. As such Virgo constitutes a formidable source for detailed observations facilitated by its proximity. However, the diversity of clusters complicates the comparisons on a one-to-one basis. Simulated clusters must be carefully selected, a daunting task since most properties are unknown. Alternatively, lookalikes produced in the proper large-scale environment can be used. Additionally, their statistical study give access to the mean properties of the observed cluster including its most probable history as well as its deviation from an average cluster. This paper presents such a statistical study with 200 Virgo-like and 400+ cluster-size random dark matter haloes. Only 18 per cent (0.5 per cent) of these random haloes comply within $3(2)\sigma$ with the mean values (radius, velocity dispersion, number of substructures, spin, velocity, concentration, centre of mass offset with respect to the spherical centre) of Virgo haloes at $z = 0$ and abide by a similar merging history up to redshift 4. None are within 1σ because of environmentally induced properties (number of substructures and velocity). For further comparisons, random haloes are selected to reproduce the mass distribution of the lookalikes to cancel mass bias effects. Redshift 1 appears then as a turning point: random to Virgo-like property ratios are alternatively smaller/larger than 1. This highlights the importance of studying clusters within their proper large-scale environment: simulated galaxy population, grandly affected by the cluster history, can then be compared with the observed one in details. Direct lookalikes simplify grandly the challenge.

Key words: methods: numerical – techniques: radial velocities – galaxies: clusters: individual.

1 INTRODUCTION

While galaxy clusters, as powerful cosmological probes, are extensively studied both observationally and numerically, comparing the observed and simulated clusters in detail can be quite challenging. The diversity of clusters in terms of morphologies, formation history, etc. (Struble & Rood 1988) indeed makes one-to-one comparisons a daunting task. The parameters that a numerical cluster should reproduce to be considered as an accurate lookalike of a given observed cluster are simply difficult to completely determine because of various aspects: lack of accuracy, no technique, or weak knowledge of the correlation between parameters. In order to take up the challenge, we propose to focus on our nearest cluster neighbour: the Virgo cluster of galaxies. Because of its proximity, this cluster has been and is still studied through numerous observational projects (e.g. Binggeli & Huchra 2000; Wong & Kenney 2009; Fritz &

Hevics Collaboration 2011; Roediger et al. 2011a; Roediger et al. 2011b; Ferrarese et al. 2012; Taylor et al. 2012; Vollmer et al. 2012; Boselli et al. 2014; Corbett Moran, Teyssier & Lake 2014; Karachentsev et al. 2014; Pappalardo et al. 2015; Boselli et al. 2016; Ferrarese et al. 2016; Lee et al. 2016; for a non-exhaustive list).

The novelty of the present paper is to conduct a numerical statistical study of the properties of the Virgo cluster via a sample of unique Virgo candidates from constrained simulations of the local Universe (e.g. Bertschinger 1987; Gottlöber, Hoffman & Yepes 2010; Lavaux 2010; Heß, Kitaura & Gottlöber 2013; Wang et al. 2016). These simulations differ from typical simulations (e.g. Alimi et al. 2012; Angulo et al. 2012; Dubois et al. 2016) in the sense that they stem from initial conditions that have been constrained with local observational data. In our case, these observational data are radial peculiar velocities (e.g. Mathewson, Ford & Buchhorn 1992; Willick et al. 1997; Zaroubi et al. 2001; Springob et al. 2007; Tully et al. 2008, 2013; Tully, Courtois & Sorce 2016), but they can also be densities obtained with redshift surveys (e.g. Skrutskie et al. 2006; Aihara et al. 2011; Lavaux & Hudson 2011; Huchra et al. 2012). The

* E-mail: jenny.sorce@univ-lyon1.fr

constrained initial conditions for these simulations are constructed with different techniques either forwards (e.g. Kitaura & Enßlin 2008; Jasche & Wandelt 2013; Kitaura 2013; Wang et al. 2014) or backwards (e.g. Dekel, Bertschinger & Faber 1990; Hoffman & Ribak 1991, 1992; Ganan & Hoffman 1993; Bistolos & Hoffman 1998; Zaroubi, Hoffman & Dekel 1999; Lavaux et al. 2008; Lavaux 2016). As a result, the simulations resemble the local Universe within a hundred megaparsecs down to a few megaparsecs (e.g. Sorce et al. 2016b).

Based on a backwards scheme described hereafter, applied to peculiar velocities, our simulations always host a unique dark matter halo, lookalike of the Virgo cluster (position, mass, velocity, etc.), in a large-scale environment that reproduces the local environment (Sorce et al. 2016a). Unlike numerical studies of clusters based on random simulations (e.g. Martizzi, Teyssier & Moore 2012; Grossauer et al. 2015; Le Brun et al. 2016; Sembolini et al. 2016; Barnes et al. 2017; Donnert et al. 2017; Hahn et al. 2017; Planelles et al. 2017), this work allows studying statistically a given cluster, here Virgo, in its proper large-scale environment. As a result of being in their proper environment, these dark matter haloes present the same quiet merging history within the past 7 gigayr (Sorce et al. 2016a) with, on average, only one merger larger than about a 10th of their mass at redshift zero within the last 4 gigayr (Olchanski & Sorce 2018). This last simulation-based finding has recently been supported by an observational study (Lisker et al. 2018). Since galaxy populations are not only sensitive to the large-scale environment of the cluster (Einasto et al. 2014) but also to its formation history, in particular its past mergers (Deshev et al. 2017), such properties are fundamental requisites to legitimize comparisons between observed and simulated galaxy populations down to the details (Grossauer et al. 2015).

This paper starts with a description of the new large sample of 200 constrained cosmological simulations run to obtain the Virgo-like sample of dark matter haloes at the core of this study. Random runs are also required to give a twofold goal to this paper. They supply random haloes within the same mass range as the Virgo-like haloes to be compared with. Subsequently, the third section explores the distribution of various properties (such as velocity, spin, number of substructures, etc.) of the 200 Virgo-like haloes as well as the evolution of these properties across cosmic time. The properties of the Virgo cluster are statistically determined. The fourth section compares random and Virgo haloes. Properties of the Virgo cluster that are constrained and/or atypical on average are highlighted. The probability to find a Virgo-like cluster given the Planck standard cosmological model and the properties that discriminate the Virgo cluster from other clusters are determined.

2 SIMULATIONS

All the dark matter simulations are run with the adaptive mesh refinement code RAMSES (Teyssier 2002) within the Planck cosmology framework ($\Omega_m = 0.307$, $\Omega_\Lambda = 0.693$, $H_0 = 67.77 \text{ km s}^{-1} \text{ Mpc}^{-1}$, $\sigma_8 = 0.829$, Planck Collaboration 2014). The resolution is set for haloes to be constituted of a minimum of 10 000 particles at redshift zero. Considering Virgo to be more massive than $10^{14} h^{-1} M_\odot$, it is equivalent to a particle mass of about $10^9 h^{-1} M_\odot$. The initially coarse grids are adaptively refined down to $3.8 h^{-1} \text{ kpc}$. Such a resolution allows us to probe also higher redshifts than zero. Simulations are run from redshift 120 to redshift zero. Note that the N -body code used in this paper is different from that used in our previous papers (e.g. Sorce et al. 2016b) for two reasons: (1) results obtained with two different N -body code are

supposed to be similar in the dark matter case only (Elahi et al. 2016). We check that this is indeed the case for our constrained simulations; (2) in a perspective of hydrodynamical simulations of the Virgo cluster, the adaptive mesh refinement grid code will be used. It is, thus, appropriate to use it to select the candidates from the sample of 200 haloes that will be run with gas.

2.1 Constrained simulations

Before running the simulations where the Virgo-like haloes can be found, initial conditions, constrained by observational data (in our case galaxy peculiar velocities) for the resulting simulations to resemble the local Universe, must be prepared. The different steps of the whole scheme used to build this set of constrained initial conditions are described in detail in Sorce et al. (2016b).

A brief description of these steps and their purpose are reminded here:

(i) Grouping of the radial peculiar velocity catalogue to remove non-linear virial motions (e.g. Tully 2015b,a) that would affect the linear reconstruction obtained with the linear method (e.g. Sorce & Tempel 2017; Sorce, Hoffman & Gottlöber 2017). Namely, when measurements are available for several galaxies in a given cluster, these measurements are replaced by one measurement, that for the cluster.

(ii) Minimizing the biases (Sorce 2015) in the grouped radial peculiar velocity catalogue. Biases are indeed inherent to any observational catalogue and in this particular case give rise to a spurious overall infall on to the local volume.

(iii) Reconstructing the 3D cosmic displacement field with the Wiener filter technique (linear minimum variance estimator, in abridged form WF, Zaroubi et al. 1995, 1999) applied to the radial peculiar velocity constraints.

(iv) Relocating constraints to the positions of their progenitors using the Reverse Zel'dovich Approximation and the reconstructed cosmic displacement field (Doumler et al. 2013), and replacing noisy radial peculiar velocities by their 3D WF reconstruction (Sorce et al. 2014). Subsequently, one can expect structures to be at the proper position, i.e. at positions similar to those observed, at the end of the simulation run.

(v) Producing density fields constrained by the modified observational peculiar velocities combined with a random realization to restore statistically the ‘missing’ structures. The WF indeed goes to the null field in absence of data or in presence of very noisy data. The constrained realization technique (CR, Hoffman & Ribak 1991, 1992), that differs schematically from the WF by a random realization added to the constraints, is used for that step. Note that this field is the first source of residual cosmic variance between the simulated Virgo haloes.

(vi) Rescaling the density fields to build constrained initial conditions and eventually increasing the resolution by adding small-scale features (e.g. MUSIC code, Hahn & Abel 2011). These small-scale features are the second source of variance between the Virgo haloes, but only at the non-linear level.

To avoid periodicity problems in the local Universe-like region, the boxsize for the 200 constrained simulations is set to $500 h^{-1} \text{ Mpc}$ at $z = 0$ (Sorce et al. 2016b). To decrease the computational cost of the 200 runs and since our interest lays solely in the study of the Virgo cluster, the zoom-in technique, first proposed by Bertschinger (2001) and implemented in MUSIC, is used. The zoom-in technique consists in keeping the large-scale environment at low resolution for its effect on the region of interest, while the resolution is increased

solely in this region. This requires knowing the position of the particles of the Virgo progenitors and their surroundings in the initial conditions.

We then proceed as follows to minimize the computational cost:

(i) The 200 constrained initial conditions are run at a low resolution (256^3 particles, i.e. a particle mass of $6 \times 10^{11} h^{-1} M_{\odot}$ or about 100 particles per Virgo-like haloes at redshift zero). At this stage, we are only interested in getting the particles that constitute Virgo and its surroundings within a $10 h^{-1}$ Mpc radius sphere to trace them back to the initial redshift in order to get their initial position. This resolution is then sufficient.

(ii) The Virgo lookalike is identified in each one of these simulations using the list of haloes obtained with Amiga's Halo Finder¹ (Knollmann & Knebe 2009).

(iii) Particles within a $10 h^{-1}$ Mpc radius sphere around the centre of the candidates are traced back to the initial redshift. They define the zoom-in region given to MUSIC to produce the initial conditions with a higher resolution in that region than in the rest of the box.

(iv) After running MUSIC with an effective resolution of 2048^3 particles for the highest level (particle mass $1.2 \times 10^9 h^{-1} M_{\odot}$), the zoom-in initial conditions are run with RAMSES and analysed with the Amiga's Halo Finder.

(v) After building the merger tree of the Virgo-like haloes, the evolution of their properties across cosmic time are stored.

2.2 Random simulations

For reference, we run 3 random initial conditions prepared with MUSIC with 1024^3 particles within a full $250 h^{-1}$ Mpc box. This box size and this number of particles ensure the same mass resolution (particle mass $1.2 \times 10^9 h^{-1} M_{\odot}$) for both the random and the Virgo-like haloes.

In these three simulations, a total of about 400+ haloes have a mass above $1.5 \times 10^{14} h^{-1} M_{\odot}$ (mass of the smallest Virgo-like halo among the 200 available), but below $10^{15} h^{-1} M_{\odot}$ (reasonable mass upper limit for the Virgo cluster, e.g. Karachentsev & Nasonova 2010; Nasonova, de Freitas Pacheco & Karachentsev 2011; Karachentsev et al. 2014; Tully 2015b) using the 'M₂₀₀' definition² (i.e the mass enclosed in a sphere with a mean density of 200 times the critical density of the Universe). Hereafter, these random haloes are referred to as cluster-size random haloes.

This cluster-size random halo sample is however biased towards the low-mass end when compared to that of the Virgo-like. To remove mass bias effects from the comparisons, an additional selection criterion is applied to the sample of cluster-size random halo. The random sample should follow a similar mass distribution as that of the Virgo halo; in other words, we set the mass distribution, $M_{0,s}^s$, of the random sample. To that end:

1) Random haloes are selected to have masses between $[\overline{M}_{0,\text{virgo}} - n \times \sigma_{M_{0,\text{virgo}}}, \overline{M}_{0,\text{virgo}} + n \times \sigma_{M_{0,\text{virgo}}}]$ where $n = 2, \sigma_{M_{0,\text{virgo}}}$ is the standard deviation of the Virgo-like masses, and $\overline{M}_{0,\text{virgo}}$ the average mass of the Virgo-like haloes at redshift zero.³ This selection permits removing extreme cases from the subsample.

2) The distribution is then forced to have the same mean and standard deviation as that of the Virgo haloes at redshift zero. The low-mass end of the subsample needs then to be resampled since there is an excess of low-mass haloes. Namely, only a few of the lower mass random haloes are randomly selected among the random haloes at the low-mass end. The random and constrained M_0 then match each other in terms of mean and standard deviation. The other moments (skewness and kurtosis) of the two distributions, in addition to be small, are found to be both of the same order of magnitude and same sign. Consequently, the distribution can be considered similar. Note that the few randomly selected haloes among the random haloes at the low-mass end alter neither the results nor the conclusions.

This strategy allows us to get a mass-unbiased sample of random haloes while preserving a high enough number of haloes for statistical purposes. Still such a selection drastically reduces the number of random haloes available for comparisons: Only 77 haloes (18 per cent) are left in the random sample, giving already an idea of the commonness of Virgo-like haloes.

3 PROPERTIES OF THE VIRGO CLUSTER WITH CONSTRAINED SIMULATIONS

Fig. 1 shows $20 h^{-1}$ Mpc XY supergalactic slices with a $5 h^{-1}$ Mpc thickness of six Virgo haloes. Boxes are oriented in the same way as the local Universe to identify the X, Y, and Z supergalactic coordinates. The gradient of colours stands for the dark matter density field. The visual similarities (positions, filaments, and their orientations) between the different Virgo haloes are already impressive compared to typical simulations of random clusters.

Fig. 2 gives the joint distributions as well as the normalized distributions of the parameters of the Virgo haloes at redshift zero in red. The black colour stands for the random haloes. Joint distributions are obtained with covariance matrices. Given that the third and fourth moments of the random and constrained parameter distributions are of the same order of magnitude and of the same sign, the use of covariance matrices is legitimate in a first approximation for simple visual comparisons. This figure is further analysed for the sole Virgo cluster in the following in two steps: (1) observed versus simulated properties, (2) statistically derived properties of the Virgo cluster from the constrained simulations.

3.1 Observed versus simulated Virgos: General agreement

Mean and standard deviation (1σ) of the normalized distributions are indicated, respectively, by red dashed and dotted lines. The blue filled circles on these normalized distributions stand for observational or reconstructed estimates of the properties of the Virgo cluster. The mass and the radius are from Shaya et al. (2017). The mass is obtained with a first turn around radius study and is thus converted to M_{200} using a 0.7 factor (Sorice et al. 2016a) and $H_0 = 67.77 \text{ km s}^{-1} \text{ Mpc}^{-1}$ (Planck cosmology). The radius is that of collapsed matter (roughly equivalent to the virial radius). It is converted to R_{200} using a 0.8 factor (obtained when comparing R_{200} and R_{vir} derived by the Halo finder and assuming that observational and numerical definitions of the virial radius give similar results). The line-of-sight velocity dispersion, dispersion of the velocity of the galaxies belonging to the cluster around their mean velocity projected along the line-of-sight direction, (Tully 2015b) is multiplied by $\sqrt{3}$ assuming a fairly isotropic dispersion.

¹Note that first, RAMSES outputs are converted to GADGET format so that they can be processed by the halo finder.

²Since results and conclusions drawn from the halo samples are identical using either the 'M₂₀₀' definition or the virial definition, we choose to present only those obtained with the 'M₂₀₀' definition.

³Note that $n = 1$ or $n = 3$ give the same results.

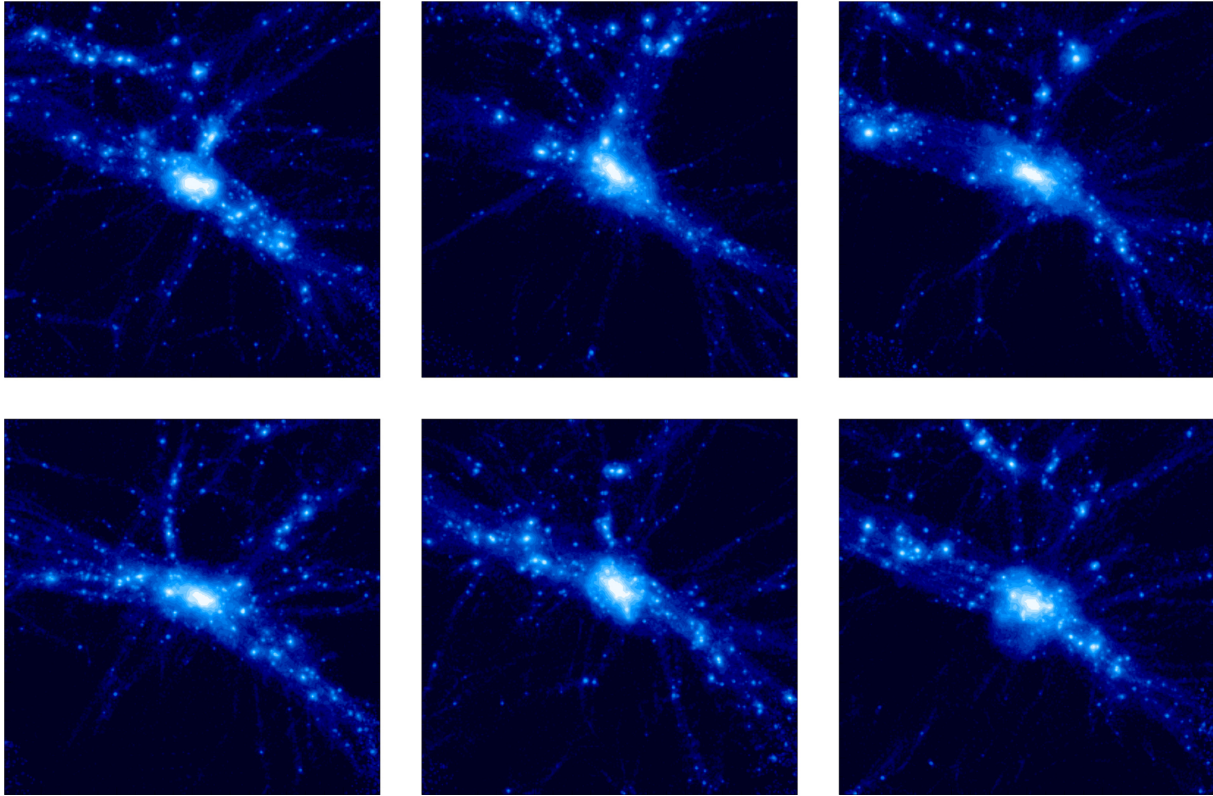


Figure 1. $20 h^{-1}$ Mpc XY supergalactic slices of $5 h^{-1}$ Mpc thickness representing six Virgos. The constrained boxes are oriented in the same way as the local Universe to obtain the X, Y, and Z coordinates. The similarities (positions, filaments, orientation, etc.) between the six Virgo haloes is remarkable. Two Virgo haloes have been selected because the values of the eight properties mentioned in Fig. 2 match the entire set of Virgo haloes’ mean property values. One Virgo halo has been selected because its merging history matches the mean merging history of the Virgo set. The other three have been completely randomly extracted from the 200 Virgo-like haloes sample.

The velocity of the cluster with respect to the CMB, hereafter velocity, is reconstructed with the WF (Sorce 2015). Other property observational estimates are not available except perhaps the number of substructures. However this would require a more detailed study especially to retain only the substructures of a given mass. That would permit also further studies including the position, merging history, population of the substructures, etc. (Boselli et al. 2014). We thus post-pone this study to another paper.

Regardless, the agreement between observational or reconstructed (blue) and simulated (thick red dashed line for the mean) estimates are remarkable given the numerous assumptions and the difficulty in comparing observed uncertain estimates and simulated properties.

3.2 Simulated Virgos: Statistically determined properties of the cluster

Furthermore, in Fig. 2 each red filled circle and ensemble of three ellipses stand, respectively, for the mean and 1 , 2 , and 3σ probabilities of the joint distributions. The panel on the top right corner is a zoom of the first panel of the fourth row of the main plot.

Expected correlations appear clearly between the mass, the radius, the velocity dispersion, and the number of substructures. Another less expected correlation is visible between the mass (or radius, number of substructures, velocity dispersion) and the offset with respect to the centre of mass: the more massive the Virgo cluster is the larger the offset is. Other much weaker correlations

between the NFW concentration (R_{halo}/r_s with R_{halo} , the radius of a halo and r_s , the break radius between an inner r^{-1} density profile and an outer r^{-3} profile; see Prada et al. 2012) and the number of substructures, or the offset between the spin and the number of substructures or the offset seem to arise. Finally, Table 1 summarizes the statistically derived values of the properties of the Virgo cluster.

4 SPECIFICITIES AND PROBABILITY OF THE VIRGO CLUSTER

4.1 Virgo-like versus random haloes

In Fig. 2, the black colour stands for the property distributions of the random halo sample with M_0^s . By construction the mass distributions of random and constrained haloes are very similar in the first row. Some obvious differences appear between the random and the constrained normalized and joint property distributions. The most interesting differences appear for the number of substructures, the offset with respect to the centre of mass, the velocity, and, to a smaller extent, the spin.

Before any further quantitative comparisons, we define two parameters relevant to determine whether a property is (a)typical or/and (not) constrained. A property is atypical if the mean value of the property for the random sample is significantly different from that obtained for the constrained sample. A property is constrained if the standard deviation of the property is larger in the random

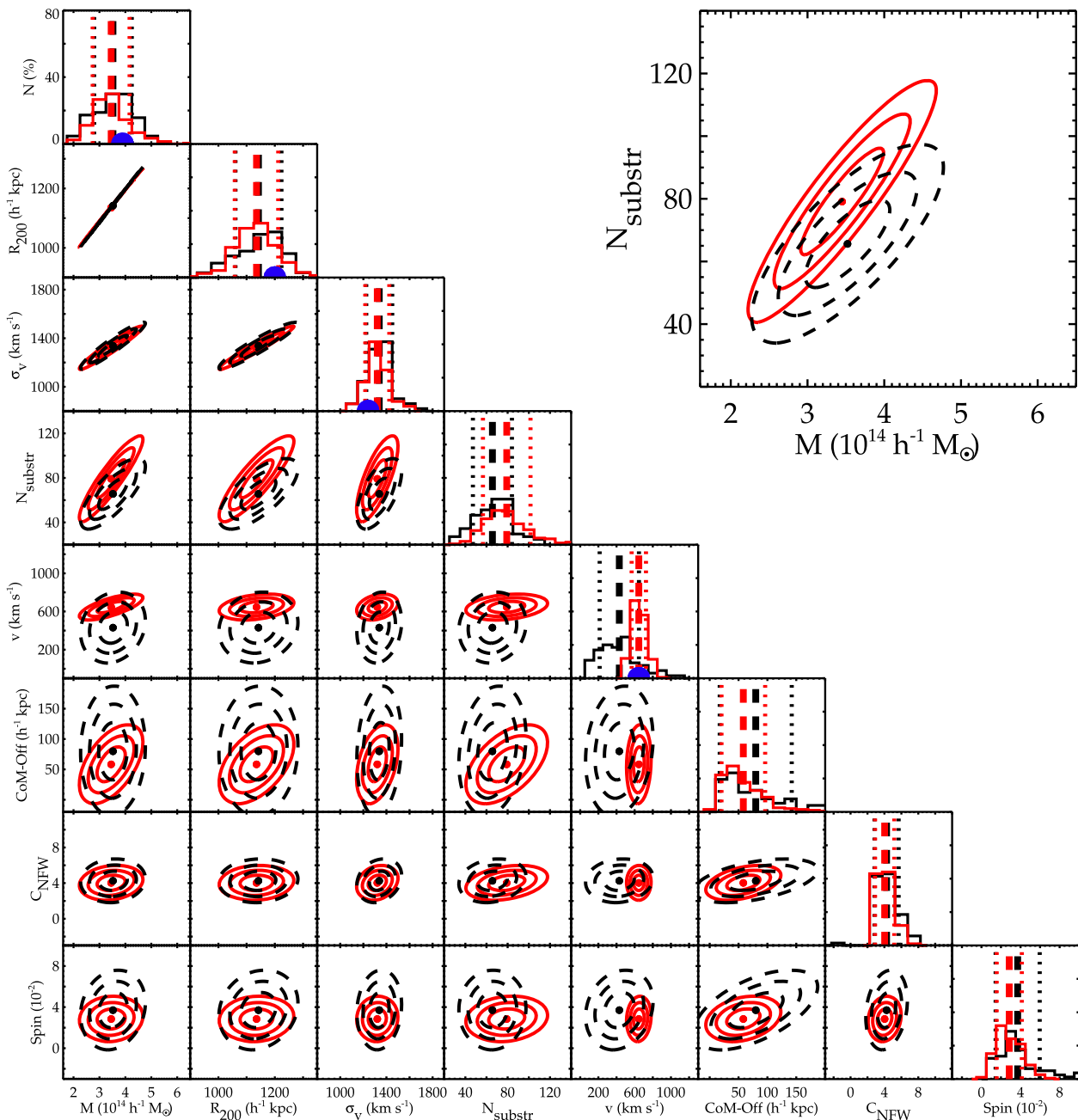


Figure 2. Normalized and joint property distributions of the mass-unbiased random halo sample (black) and Virgo halo sample (red). Thick dashed and thin dotted lines stand for the mean and standard deviation of the normalized distribution using the same respective colours. The filled circles and the ensemble of three ellipses are the mean and 1, 2, and 3σ probabilities of the joint distributions. Random haloes have masses between $[\overline{M}_{0,\text{virgo}} - 2 \times \sigma_{M_{0,\text{virgo}}}, \overline{M}_{0,\text{virgo}} + 2 \times \sigma_{M_{0,\text{virgo}}}]$ where $\sigma_{M_{0,\text{virgo}}}$ is the standard deviation of the Virgo-like masses and $\overline{M}_{0,\text{virgo}}$ is the mean mass of the Virgo-like haloes at $z = 0$. The blue filled circles on the normalized distributions are observational or reconstructed estimates of the properties of the observed Virgo cluster. From left to right or top to bottom, properties are mass, radius, velocity dispersion, number of substructures, velocity, centre of mass offset with respect to the spherical centre, concentration, and spin.

case than in the constrained case. Note that theoretically if the property is atypical, it can also be considered as constrained, but for the sake of clarity these two concepts are distinguished in the rest of the paper. It can happen that both conditions are fulfilled then the property is both constrained and atypical. To measure these conditions quantitatively, we use the formula given in equation 1 (the larger in absolute value Δ is, the more significantly different the means are) and the ratio of the constrained (virgo) and random (rand) standard deviations (the smaller with respect to 1 the ratio is,

the more constrained the studied parameter is), respectively.

$$\Delta = \frac{\overline{X}_{\text{virgo}} - \overline{X}_{\text{rand}}}{\sqrt{\sigma_{\text{virgo}}^2/n_{\text{virgo}} + \sigma_{\text{rand}}^2/n_{\text{rand}}}}, \quad (1)$$

where n is the number of haloes in the considered sample, σ the standard deviation, and \overline{X} the mean. Δ is given in standard error units. Typically, definitions used in the following are : (1) if Δ in absolute values is larger than 3 (9) standard error units, then it means

Table 1. Statistically derived values of the properties of the Virgo cluster.

Parameter	Mean	Standard deviation
M_{200} ($h^{-1} M_{\odot}$)	$3.45e + 14$	$7.1e + 13$
R_{200} (h^{-1} kpc)	1135	77
σ_v (km s^{-1})	1321	104
$N_{\text{substr}} (M > 1e + 10)$	79	22
v (km s^{-1})	646	79
CoM-off (h^{-1} kpc)	58	38
C_{NFW}	4	1
Spin	0.03	0.01

that the two means differ significantly / at 99.9 per cent (extremely significantly / quasi at 100 per cent); (2) If the ratio of the standard deviations is smaller than 0.95 (0.55), the range of possible values for a given property of Virgo-like haloes is divided by more than 1.05 (1.8), and the property is constrained (extremely constrained).

In the following, in addition to the random or constrained comparison at redshift zero visible on Fig. 2, since the evolution might tell us more about the typicalness of the Virgo cluster, we

further probe also the links between the properties at redshifts higher than zero. We thus examine one property at a time for both the Virgo sample and the mass-unbiased random sample. Tentatively, properties are gathered in two groups: (1) the internal properties that are a priori linked namely the mass, radius, number of substructures, velocity dispersion, and to a lesser extent the concentration and (2) the external properties due a priori purely to the environment, i.e. velocity, spin, and the centre of mass offset with respect to the spherical centre.

(i) Number of substructures: the top row of the rightmost top plot in Fig. 3 shows that, before redshift 1, Virgo haloes have slightly less substructures than random haloes and after redshift 1 they have more substructures than random haloes. Apart at redshift 1, Virgo haloes tend to be atypical ($\Delta \neq 0$). The fourth row of Fig. 2 confirms that Virgo haloes have on average more substructures than random haloes with $M_{200,0}^s$ given their mass, radius, and velocity dispersion. The enlarged panel establishes the absence of mass biases between the random and Virgo samples. There is a clear signal of about 1σ . It can be attributed to the fact that the Virgo cluster is a priori not

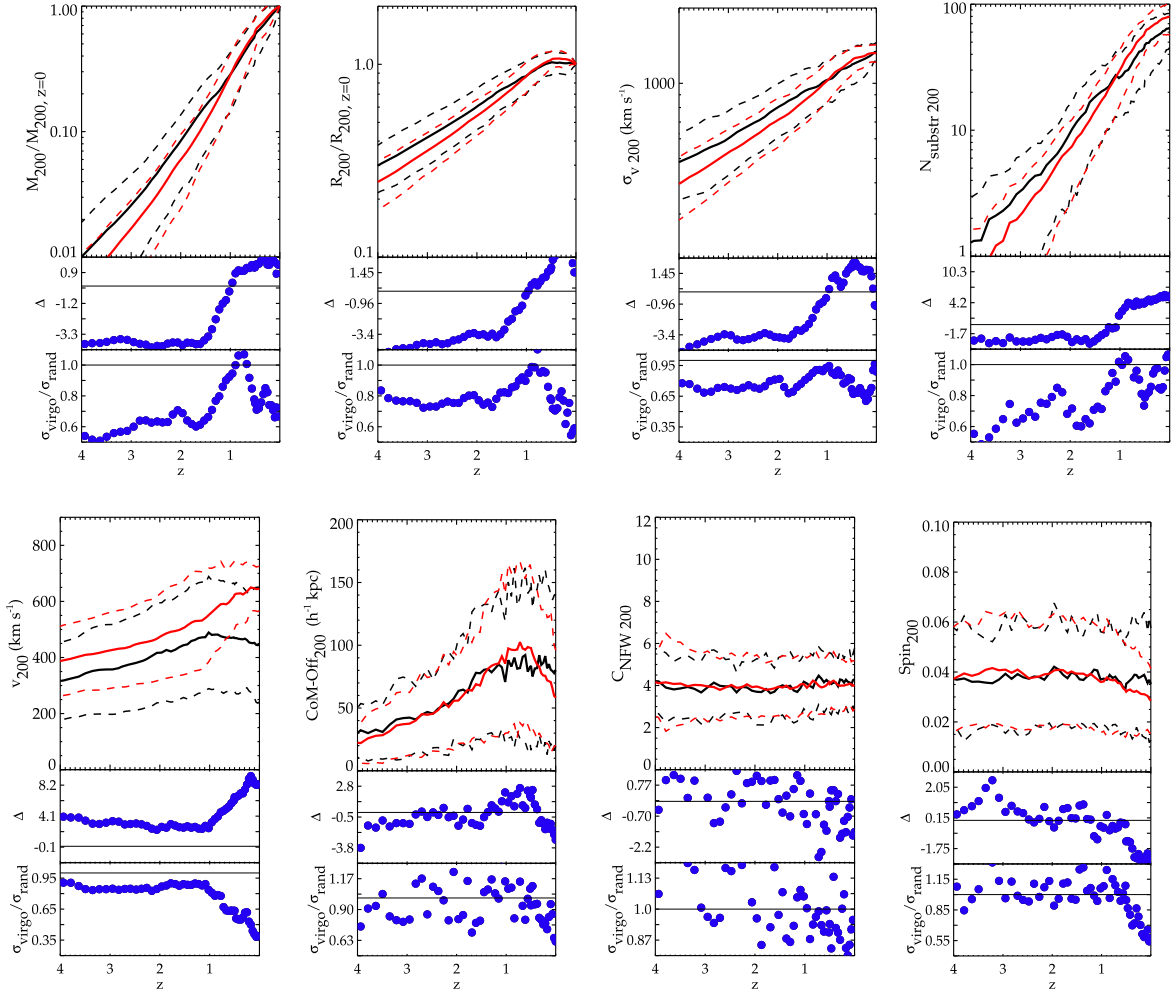


Figure 3. Top row: average property (solid line) and its standard deviation (dashed lines) as a function of the redshift for the 200 Virgo haloes (red) and for the 77 random haloes with M_0^s (black). Middle row: quantitative difference between the mean random and constrained property derived with the formula given in equation 1. The solid black line denotes the value of insignificant differences (see the text for a detailed explanation). Bottom row: ratio of the standard deviation of the constrained property to that of the random property. The solid black line delimits the constrained zone (value inferior to 1) from the unconstrained area (value greater than 1). From left to right, top to bottom, properties are mass, radius, velocity dispersion, number of substructures, velocity, centre of mass offset with respect to the spherical centre, concentration, and spin.

fully virialized. Some internal structures are still in the process of merging (Boselli et al. 2014). In addition, at every redshift larger than 1, the last row of the left plot in Fig. 3 shows that the possible range of number of substructures for Virgo haloes is about 10–20 per cent (or even 30–40 per cent in some cases) smaller than that for random haloes.

(ii) Mass and merging history: according to the top row of the extreme left top plot in Fig. 3, the mean merging history of the Virgo haloes is different from that of the selected random haloes as already noticed in Sorce et al. (2016a), but with a much smaller sample. They differ significantly ($|\Delta| > 3$) at redshift earlier than 1. Again redshift 1 seems to be a turning point for the Virgo haloes. At this redshift, their mass accretion rate decreases drastically. At later redshifts, the random and constrained mean merging histories differ moderately ($|\Delta| \sim 1$). It means that for their mass, at all redshifts, the Virgo haloes do not have a typical merging history. They had a more active history in the past than within the last 7 gigayr. This observation is in agreement with the halo-bias at fixed mass: a halo that grows in an underdensity accreted a large amount of matter at high redshifts. While somewhat boosted by another cluster in the past, the latter has to be not too close for the accretion of the cluster of interest nowadays to be very weak but not stalled (Hahn et al. 2009; Borzyszkowski et al. 2017; Musso et al. 2018). The Centaurus cluster is indeed in the vicinity, while still about $15 h^{-1}$ Mpc away from Virgo and the local Universe seems to be a general underdensity (Keenan, Barger & Cowie 2013). The link between the atypicality of the Virgo cluster merging history and its environment is established. The different past histories of the clusters are tightly entangled to their environment. In addition, except at redshift about 1, the Virgo haloes have a smaller range of possible merging histories than random haloes (ratio of the standard deviations smaller than 1). These assessments underline that getting clusters with a merging history matching that of the Virgo haloes requires several criteria.

(iii) Radius (Fig. 3, second top panel): the radius presents the exact same behaviour as the merging history, a completely expected behaviour because of its strong correlation with the mass.

(iv) Velocity dispersion (Fig. 3, third top panel): the velocity dispersion also strongly correlated to the mass is no exception. Redshift 1 appears again as a turning point.

(v) Concentration (Fig. 3, third bottom panel): it is a commendable exception as it is stable across late cosmic time for both constrained and random haloes without major differences between the two. In that respect, Virgo haloes are typical at all redshifts and not only at $z = 0$.

(i) Centre of mass offset: The top row of the second bottom plot in Fig. 3 shows the evolution of the offset of the centre of mass of the haloes with respect to their spherical centre. For both random and constrained haloes, this offset increases until a redshift approximately equal to 1. At smaller redshifts than 1, the offset decreases more or less rapidly and faster for the Virgo haloes than for the random haloes. The quiet merging history of the Virgo cluster in the last few gigayears might be the reason for such an observation. The offset tends to be slightly larger for Virgo haloes than for random haloes at redshifts close to 1. At redshift zero, constrained mean offset values are smaller than that for the random haloes in a significant way (second row of the plot). The ratio of the standard deviation is centred on 1. Namely the offset of the centre of mass is overall not constrained according to the definition chosen at the beginning of the section where we split between constrained and atypical attributes. However, interestingly Fig. 2 shows a stronger

correlation between the centre of mass offset and the mass (or radius, velocity dispersion, number of substructures) for the Virgo haloes than for the random haloes. The indirect constraint on the merging history (constraint via the large-scale environment) is probably the reason for such an observation. Basically, although there is still a residual cosmic variance in terms of mass, at a given mass the constrained history tends to favour lower offsets with respect to the centre of mass. However, with increasing mass, this offset still rises irremediably, because the most massive Virgo haloes must accrete more mass although according to the same scheme as the smallest ones in the same amount of time.

(ii) Spin (Fig. 3, last bottom panel): the spin behaves exactly like the other parameters with the change of trend at redshift 1. Note that the random and constrained mean values of the spin are always only moderately different. The ratio of the standard deviations of the constrained and random spin values is smaller than 1 by up to 45 per cent for redshift smaller than 1. Fig. 2 confirms that at redshift zero the spin of a Virgo halo has a smaller range of possible values than an average random halo. Since spin and local environment are linked, it confirms that Virgo haloes are in a well constrained environment at least within the last 7 gigayr, with no major merger.

(iii) Velocity: the behaviour of the mean velocity is shown in Fig. 3, first bottom panel. As expected, masses and velocities have no strong link. Hence, while the random haloes have an average velocity of $463 \pm 207 \text{ km s}^{-1}$, the Virgo haloes have an average velocity higher by almost 200 km s^{-1} ($646 \pm 79 \text{ km s}^{-1}$ barely within 1σ of the random distribution)⁴ at redshift zero (cf. Fig. 2). Typically, at all redshifts, the Virgo haloes have a larger velocity than the random haloes (top row) with a high level of significance (second row) and different standard deviations (third row). The latter differ significantly between redshifts 0 and 1 (last row). The ratio of the constrained and random standard deviations is always smaller than 1. As a side note, the average velocity vector direction of the Virgo halo is $(-529 \pm 78; 268 \pm 66; -236 \pm 78) \text{ km s}^{-1}$. As expected, the vector points in the direction of the great attractor and beyond, where the shapley supercluster stands.

This analysis shows us that (1) the Virgo cluster is a priori not a completely typical cluster, especially, regarding its velocity, or in other words its large-scale environment is not typical, thus it gives birth to an atypical cluster, (2) some characteristics of the Virgo cluster are statistically constrained not only at redshift zero but also at earlier redshifts. The next section aims at summarizing all these findings.

4.2 Discriminative properties of the Virgo cluster

Table 2 recapitulates the properties studied in the previous section and highlights those atypical and/or constrained, i.e. that differ (significantly) between Virgo and selected random haloes at redshift zero. As previously stated, the atypical and constrained adjectives can qualify a property if : #1 the constrained and random mean values of the property differ (significantly). Namely, equation 1 gives a non-zero and large absolute value; #2 the constrained and random property distribution have (significantly) different standard deviations with a ratio constrained to random smaller than 1. Δ and ratio values are followed either by a long dash (#1 $|\Delta| > 3$; #2 ratio < 0.95) or a frame ((#1 $|\Delta| > 9$; #2 ratio < 0.55) in the table to

⁴Note that the offset that may be induced by the different boxsizes is smaller than the standard deviation of the constrained velocities (Suhonenko & Gramann 2003)

Table 2. (1) Difference between the mean property values of the 200 Virgo haloes and of the selected random haloes / (2) ratio of the standard deviations of their properties. 1000 different draws of haloes among the cluster-size random sample have been made to estimate the variance of Δ and the ratio on the random sample drawn to match the mass distributions. A long dash (frame) highlights an (a highly) atypical / constrained property value (according to equation 1, absolute values above 3 and 9 in standard error units, or values below 0.95 and 0.55, respectively) for the Virgo haloes with respect to selected random haloes.

	(1)	(2)	
R_{200}	-0.44 ± 0.21	0.91 ± 0.03	–
σ_v	-0.79 ± 0.28	0.87 ± 0.04	–
N_{substr}	5.36 ± 0.14	1.2 ± 0.04	–
v	8.10 ± 0.53	0.38 ± 0.01	□
CoM-off	-2.69 ± 0.32	0.62 ± 0.01	–
C_{NFW}	-1.40 ± 0.40	0.81 ± 0.03	–
Spin	-2.30 ± 0.41	0.62 ± 0.05	–

highlight the different or extremely different values. The standard deviations of these values are obtained by drawing 1000 times haloes among the cluster-size haloes to get samples that match the mass distribution of Virgo haloes at $z = 0$. We hereafter give examples of properties fulfilling condition #1, condition #2 or both conditions:

(i) If the random haloes are selected according to their mass (column (1) of Table 2), then Virgo haloes are atypical in terms of their number of substructures and velocity in the sense that their mean values fulfil condition #1.

(ii) According to condition #2, although Virgo haloes have overall typical centre of mass offset, concentration, and spin values, their range of possible values is smaller than that of the random haloes selected upon their masses as shown in column (2) of Table 2.

(iii) The line (5) of table 2 shows that the velocity fulfils the two conditions. This is not unexpected since the simulations all resemble the local Universe. The reproduced local large-scale structure then induces the same motion for all the Virgo haloes. However, the low probability for random haloes to have the same motion as Virgo haloes indicates the low probability to have a local environment inducing this velocity.

According to this table the most atypical property of the Virgo haloes at $z = 0$ is their velocity. Their number of substructures is also not quite typical but to a lesser extent. If given their masses, Virgo haloes have globally more substructures than random haloes; it is not as significant as the atypicality of their velocity. On the contrary, the concentration is the less atypical value and the number of substructures is the less constrained one, although a more detailed study is required here to quantify the masses of these substructures.

This table is valid at redshift zero. It would be fastidious to present it at all redshifts. Instead, Fig. 4 gives a visual overall impression of the status (atypical or/and constrained) of the properties at different redshift. Δ and the ratio of the constrained and random standard deviations are derived for each property under study at different redshifts (one colour per redshift).

Links between the different properties are visible. For instance, as expected the radius is quite typical. More importantly redshift 1 appears clearly as the redshift of changes: the light blue filled squares stand out between the symbols used for the earliest redshifts and those used for the latest redshifts. For instance, R_{200} , σ_v , and N_{substr} are atypical at $z > 0$, but at $z = 1$: from large values at $0 < z < 1$, Δ becomes quasi-null at $z = 1$ to increase again in

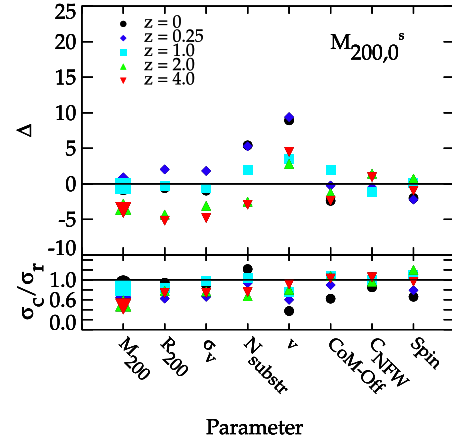


Figure 4. Quantitative measurement of the difference between the mean property values of the 200 Virgo haloes and of the selected random haloes (top row, equation 1) as well as the ratio of their standard deviations (bottom row). The mass distribution of the random haloes is matched (thus plotted as the largest symbol) to that of the Virgo haloes. Measurements are given at different redshifts (coloured symbols) in all the panels.

absolute value. To conclude, most of Virgos' properties appear to be atypical and/or constrained at various levels at all redshifts but 1.

So far, random haloes have been selected only on their mass and an additional criterion was added to their mass distribution. It is interesting to take a step back to see how many random haloes have property values that all fall within 3σ of Virgos' values at redshift zero without the additional criterion, i.e. considering the 400+ random halo sample. We first check how many of the Virgo haloes are in their own 3σ scatter simultaneously for the 8 properties under study in this paper. 97 per cent of the Virgo haloes comply with this request. By comparison, only 30 per cent of the random haloes are left. Virgo is thus an unlikely cluster of galaxies nowadays and by extension at earlier redshifts: until at least redshift 1, the redshift of the changes.

To understand which property is responsible for this huge drop in the number of haloes besides the constraint on their mass (they need to be cluster-size haloes), it is then interesting to add an additional selection criterion. This additional criterion consists either in matching successively a given parameter distribution of the selected random haloes to that of the Virgo haloes or in simply restricting the range parameter values to $[\bar{X}_{0,\text{virgo}} - 2 \times \sigma_{X_{0,\text{virgo}}}, \bar{X}_{0,\text{virgo}} + 2 \times \sigma_{X_{0,\text{virgo}}}]$, where $\sigma_{X_{0,\text{virgo}}}$ is the standard deviation of the Virgo-like X property and $\bar{X}_{0,\text{virgo}}$ is the mean X property of the Virgo-like haloes at $z = 0$. The appendix gathers the results for the different additional selection criteria. Selecting the cluster-size random haloes on the additional velocity distribution criterion is the major cause of decrease in the number of random haloes left (16 per cent, 49 per cent restricting only the range of velocity without reproducing the distribution). This observation then tends to imply that our local environment is quite atypical. Moreover, Fig. 5 shows that two additional criteria to match the cluster-size random haloes' velocity and mass distributions to that of the Virgo haloes is not sufficient to get the proper number of substructures.

Furthermore, adding the third criterion consisting in matching the distribution of the numbers of substructures of the random haloes to that of the constrained haloes does not give solely random haloes that have a quiet merging history within the last 7 gigayr (i.e. they had a major merger within the last 7 gigayr, their masses grew rapidly). With the more relax range restriction rather than

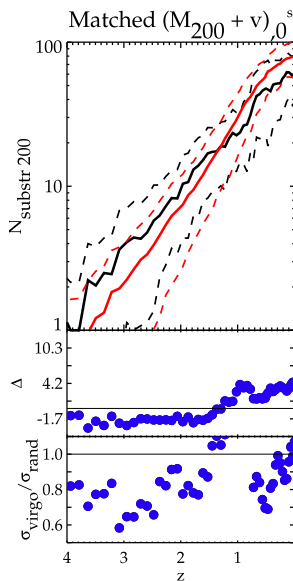


Figure 5. Same as Fig. 3, but random haloes are selected so as to match both their mass and velocity distributions to those of the Virgo haloes.

distribution matching criterion on mass, velocity, and number of substructures, only 18 per cent (0.5 per cent) of these random haloes have merging histories within $3(2)\sigma$ of that of the Virgo haloes. None are within 1σ . This implies that merging histories are not defined solely by the properties under study in this paper (although the velocity linked to the environment is considered). Reversely, the merging history type constrains some parameters. Studying the impact of the environment on merging histories to find the type of environments leading to merging histories similar to Virgo haloes will shed some light on the environment we are living in. The essential peculiarities of the latter for having a Virgo cluster with such a merging history can be highlighted. Such a study that requires a huge halo sample for statistical purposes is underway. It will also focus on the redshift of change, $z = 1$. Actually, several turning points are known to occur during the formation of the dark matter haloes for different reasons, like for instance when their concentration reaches a given value at $z > 4$ (Zhao et al. 2003). This paper highlights yet another turning point that occurs at about half the Universe’s age indicating that there are most probably, in a first approximation, two types of environment giving two types of halo merging histories intersecting at about $z = 1$. The mean merging history of the random haloes gives the average between two types of merging histories: one like the Virgo haloes with major accretion in the past and a recent slowdown, another with minor accretion in the past and a recent increase. However, the current number of random haloes is insufficient to confirm definitively this hypothesis. Still, note that this hypothesis and the observations are in full agreement with the halo-bias at fixed mass described in 4.1.

5 CONCLUSION

Galaxy clusters are powerful cosmological probes. Combined with their numerical complement that emerged within the past few years, they permit studying the formation and evolution of clusters and testing theoretical models. As such Virgo constitutes a formidable source of information via detailed observations facilitated by its proximity with us. However, accessing all the properties and the past history of the cluster from nowadays observations to select the numerical lookalike valid for a one-to-one detailed comparison

is not completely trivial. A wide variety of existing clusters, most probably a result of an environmental diversity, complicates the detailed comparisons on a one-to-one basis.

At this stage, accurate lookalikes of the Virgo cluster come in handy to determine the properties of the Virgo cluster, its likeliness, and thus its environmental likelihood, as well as to supply the numerical complement. We obtain 200 of such Virgo-like haloes by applying the zoom-in technique to 200 constrained initial conditions. By definition of a constrained simulation, the Virgo haloes formed in a reproduction of our local environment. These simulations have been proven in the past (but only with a very limited sample size) to give accurate reproductions of the Virgo cluster in general (i.e. mass, position, and merging history). Besides conducting a thorough statistical study of these 200 haloes, we compare them to random haloes extracted from a set of three random simulations with the same (resolution and cosmological framework) features as those used for the Virgo haloes.

Random haloes are selected so that their mass distribution reproduces that of the Virgo haloes. Results and conclusion are unaffected by the set of selected random haloes. Two appellations are used to characterize a given property: a property can be considered (1) atypical or/and (2) constrained. It is atypical if its average value obtained for the Virgo haloes differ (significantly) from that obtained for the random haloes. It is constrained if its standard deviation is (significantly) smaller for Virgo haloes than for random haloes. Studies are conducted at different redshifts.

Conclusions are as follows for a set of random haloes sharing the same mass distribution as that of the Virgo haloes:

(i) As expected by definition of a constrained simulation valid down to the cluster scale, most of the properties of the Virgo haloes are constrained with respect to those of the random haloes at all redshifts. The only exception is the number of substructures for redshift smaller than 1. A more detailed analysis of these substructures (masses, positions) will follow.

(ii) Until about 7.8 gigayr ago ($z = 1$), the trends of most properties of the Virgo haloes with respect to those of the random haloes were reversed with respect to today; property values that were larger (smaller) for Virgo haloes than for random haloes became smaller (larger) at $z = 1$. Hence, Virgo haloes have on average a larger number of substructures, a quieter merging history nowadays than random haloes, sharing the same mass distribution as them at $z = 0$, while it was the opposite at redshifts larger than 1. The environment is probably the cause for such an observation. This reinforces the necessity to simulate clusters in the proper environment to push further the comparisons with observed ones.

(iii) Required but not sufficient criteria to select random haloes that match Virgo haloes are the mass (or alternatively the radius) and the velocity at $z = 0$. These two criteria ensure that radius (mass), velocity dispersion, concentration, and spin are shared between random and Virgo haloes at redshift zero on average. However, the offset of their centre of mass with respect to the spherical centre is not constrained and their numbers of substructures are about 1σ away. Obviously the random merging histories are not all quiet. The velocity is a necessary but not sufficient condition to get the proper environment even if it is correlated on large scales.

(iv) A third requirement to select a perfect candidate for the Virgo cluster will then be for instance the number of substructures. However, even if the random haloes have values within 3σ of the average Virgo values, the merging history of random haloes still differs from that of Virgo haloes on average. These selection criteria are efficient only at $z = 0$. The merging history itself can then be considered as a criterion.

(v) Nevertheless, getting a random halo that matches the Virgo cluster is a daunting task. Only 18 per cent (0.5 per cent) of the random haloes have their eight properties (mass, radius, velocity dispersion, number of substructures, concentration, offset with respect to the centre of mass, velocity, and spin) within $3(2)\sigma$ of the average Virgo values at $z = 0$ and their merging history that matches within $3(2)\sigma$ that of Virgo haloes up to redshift 4. None are within 1σ . Since the merging history forged by the environment is the additional requirement, it becomes clear that simulated clusters are accurate counterparts of the observed ones only when they are simulated in the proper large scale environment.

Consequently, (1) this set of 200 Virgo haloes highlights the complexity in getting a numerical cluster that matches the observed Virgo cluster of galaxies. Such a pairing is however essential to push studies further in details. This paper gives the values of the properties to be matched especially if they affect the galaxy population of the cluster like the merging history does (e.g. Grossauer et al. 2015). Only then detailed comparisons between simulated and observed galaxy populations are legitimate to test galaxy formation and evolution models, and to calibrate them ; (2) this set of 200 Virgo haloes also opens great perspectives to lead comparisons with observations as they simplify grandly the challenge of selecting the proper simulated cluster. In particular, it will permit studying the substructures of the Virgo cluster. The impact of the environment on cluster properties can be studied in more details. The reason for the quiet merging history of the Virgo cluster within the last seven gigayears already previously highlighted but with a much smaller statistical sample of Virgo haloes certainly deserves attention. An ongoing study with an extremely large statistical sample of haloes suggests a potential link between the type (quiet or active) of merging histories and the number of neighbours (depending on their distance and mass) at $z = 0$ and may also explain the existence of a redshift of change. Finally, a few representative Virgo haloes will be selected from this set to run zoom-in hydrodynamical simulations of the Virgo cluster that will permit testing precisely the galaxy formation and evolution models giving birth to galaxy cluster populations. In addition, the implications of having a massive neighbour for the local Group, in particular our Galaxy, might be highlighted.

ACKNOWLEDGEMENTS

The authors gratefully acknowledge the Gauss Centre for Supercomputing e.V. (www.gauss-centre.eu) for providing computing time on the GCS Supercomputers SuperMUC at LRZ Munich. JS thanks her CLUES collaborators in particular Stefan Gottlöber for useful discussions. JS acknowledges support from the ‘l’Oréal-UNESCO Pour les femmes et la Science’ and the ‘Centre National d’études spatiales (CNES)’ post-doctoral fellowship programs.

REFERENCES

Aihara H. et al., 2011, *ApJS*, 193, 17
 Alimi J.-M. et al., 2012, preprint ([arXiv:1206.2838](https://arxiv.org/abs/1206.2838))
 Angulo R. E., Springel V., White S. D. M., Jenkins A., Baugh C. M., Frenk C. S., 2012, *MNRAS*, 426, 2046
 Barnes D. J. et al., 2017, *MNRAS*, 471, 1088
 Bertschinger E., 1987, *ApJ*, 323, L103
 Bertschinger E., 2001, *ApJS*, 137, 1
 Binggeli B., Huchra J., 2000, in Murdin P., ed., *Virgo Cluster*, Encyclopedia of Astronomy and Astrophysics, Institute of Physics Publishing, Bristol, p. 1822
 Bistolas V., Hoffman Y., 1998, *ApJ*, 492, 439

Borzyszkowski M., Porciani C., Romano-Díaz E., Garaldi E., 2017, *MNRAS*, 469, 594
 Boselli A. et al., 2014, *A&A*, 570, 25
 Boselli A. et al., 2016, *A&A*, 585, 14
 Corbett Moran C., Teyssier R., Lake G., 2014, *MNRAS*, 442, 2826
 Dekel A., Bertschinger E., Faber S. M., 1990, *ApJ*, 364, 349
 Deshev B. et al., 2017, *A&A*, 607, 18
 Donnert J. M. F., Beck A. M., Dolag K., Röttgering H. J. A., 2017, *MNRAS*, 471, 4587
 Doumler T., Hoffman Y., Courtois H., Gottlöber S., 2013, *MNRAS*, 430, 888
 Dubois Y., Peirani S., Pichon C., Devriendt J., Gavazzi R., Welker C., Volonteri M., 2016, *MNRAS*, 463, 3948
 Einasto M., Lietzen H., Tempel E., Gramann M., Liivamägi L. J., Einasto J., 2014, *A&A*, 562, 14
 Elahi P. J. et al., 2016, *MNRAS*, 458, 1096
 Ferrarese L. et al., 2012, *ApJS*, 200, 42
 Ferrarese L. et al., 2016, *ApJ*, 824, 22
 Fritz J., Hevics Collaboration, 2011, in Wang W., Lu J., Luo Z., Yang Z., Hua H., Chen Z., eds, *ASP Conf. Ser. Vol. 446, Galaxy Evolution: Infrared to Millimeter Wavelength Perspective*. Astron. Soc. Pac., San Francisco, p. 77
 Ganon G., Hoffman Y., 1993, *ApJ*, 415, L5
 Gottlöber S., Hoffman Y., Yepes G., 2010, preprint ([arXiv:1005.2687](https://arxiv.org/abs/1005.2687))
 Grossauer J. et al., 2015, *ApJ*, 807, 16
 Hahn O., Abel T., 2011, *MNRAS*, 415, 2101
 Hahn O., Porciani C., Dekel A., Carollo C. M., 2009, *MNRAS*, 398, 1742
 Hahn O., Martizzi D., Wu H.-Y., Evrard A. E., Teyssier R., Wechsler R. H., 2017, *MNRAS*, 470, 166
 Heß S., Kitaura F.-S., Gottlöber S., 2013, *MNRAS*, 435, 2065
 Hoffman Y., Ribak E., 1991, *ApJ*, 380, L5
 Hoffman Y., Ribak E., 1992, *ApJ*, 384, 448
 Huchra J. P. et al., 2012, *ApJS*, 199, 22
 Jasche J., Wandelt B. D., 2013, *MNRAS*, 432, 894
 Karachentsev I. D., Nasonova O. G., 2010, *MNRAS*, 405, 1075
 Karachentsev I. D., Tully R. B., Wu P.-F., Shaya E. J., Dolphin A. E., 2014, *ApJ*, 782, 4
 Keenan R. C., Barger A. J., Cowie L. L., 2013, *ApJ*, 775, 62
 Kitaura F.-S., 2013, *MNRAS*, 429, L84
 Kitaura F. S., Enßlin T. A., 2008, *MNRAS*, 389, 497
 Knollmann S. R., Knebe A., 2009, *ApJS*, 182, 608
 Lavaux G., 2010, *MNRAS*, 406, 1007
 Lavaux G., 2016, *MNRAS*, 457, 172
 Lavaux G., Hudson M. J., 2011, *MNRAS*, 416, 2840
 Lavaux G., Mohayaee R., Colombi S., Tully R. B., Bernardeau F., Silk J., 2008, *MNRAS*, 383, 1292
 Le Brun A. M. C., McCarthy I. G., Schaye J., Ponman T. J., 2016, *MNRAS*, 466, 4442
 Lee H.-R., Lee J. H., Jeong H., Park B.-G., 2016, *ApJ*, 823, 73
 Lisker T., Vijayaraghavan R., Janz J., Gallagher J. S., III, Engler C., Urich L., 2018, *ApJ*, 865, 40
 Martizzi D., Teyssier R., Moore B., 2012, *MNRAS*, 420, 2859
 Mathewson D. S., Ford V. L., Buchhorn M., 1992, *ApJS*, 81, 413
 Musso M., Cadiou C., Pichon C., Codis S., Kraljic K., Dubois Y., 2018, *MNRAS*, 476, 4877
 Nasonova O. G., de Freitas Pacheco J. A., Karachentsev I. D., 2011, *A&A*, 532, 12
 Olchanski M., Sorce J. G., 2018, *A&A*, 614, 9
 Pappalardo C. et al., 2015, *A&A*, 573, 13
 Planck Collaboration, 2014, *A&A*, 571, 66
 Planelles S. et al., 2017, *MNRAS*, 467, 3827
 Prada F., Klypin A. A., Cuesta A. J., Betancort-Rijo J. E., Primack J., 2012, *MNRAS*, 423, 3018
 Roediger J. C., Courteau S., MacArthur L. A., McDonald M., 2011a, *MNRAS*, 416, 1996
 Roediger J. C., Courteau S., McDonald M., MacArthur L. A., 2011b, *MNRAS*, 416, 1983
 Sembolini F. et al., 2016, *MNRAS*, 457, 4063

- Shaya E. J., Tully R. B., Hoffman Y., Pomarède D., 2017, *ApJ*, 850, 15
 Skrutskie M. F. et al., 2006, *AJ*, 131, 1163
 Sorce J. G. et al., 2016b, *MNRAS*, 455, 2078
 Sorce J. G., 2015, *MNRAS*, 450, 2644
 Sorce J. G., Tempel E., 2017, *MNRAS*, 469, 2859
 Sorce J. G., Courtois H. M., Gottlöber S., Hoffman Y., Tully R. B., 2014, *MNRAS*, 437, 3586
 Sorce J. G., Gottlöber S., Hoffman Y., Yepes G., 2016a, *MNRAS*, 460, 2015
 Sorce J. G., Hoffman Y., Gottlöber S., 2017, *MNRAS*, 468, 1812
 Springob C. M., Masters K. L., Haynes M. P., Giovanelli R., Marinoni C., 2007, *ApJS*, 172, 599
 Struble M. F., Rood H. J., 1988, *Sky Telesc.*, 75, 16
 Suhhonenko I., Gramann M., 2003, *MNRAS*, 339, 271
 Taylor R., Davies J. I., Auld R., Minchin R. F., 2012, *MNRAS*, 423, 787
 Teyssier R., 2002, *A&A*, 385, 337
 Tully R. B. et al., 2013, *AJ*, 146, 25
 Tully R. B., 2015a, *AJ*, 149, 54
 Tully R. B., 2015b, *AJ*, 149, 171
 Tully R. B., Shaya E. J., Karachentsev I. D., Courtois H. M., Kocevski D. D., Rizzi L., Peel A., 2008, *ApJ*, 676, 184
 Tully R. B., Courtois H. M., Sorce J. G., 2016, *AJ*, 152, 50
 Vollmer B., Wong O. I., Braine J., Chung A., Kenney J. D. P., 2012, *A&A*, 543, 31
 Wang H. et al., 2016, *ApJ*, 831, 18
 Wang H., Mo H. J., Yang X., Jing Y. P., Lin W. P., 2014, *ApJ*, 794, 94
 Willick J. A., Courteau S., Faber S. M., Burstein D., Dekel A., Strauss M. A., 1997, *ApJS*, 109, 333
 Wong O. I., Kenney J. D. P., 2009, in Sheth K., Noriega-Crespo A., Ingalls J., Paladini R., eds, *The Evolving ISM in the Milky Way and Nearby Galaxies*. p. 66
 Zaroubi S., Hoffman Y., Fisher K. B., Lahav O., 1995, *ApJ*, 449, 446
 Zaroubi S., Hoffman Y., Dekel A., 1999, *ApJ*, 520, 413
 Zaroubi S., Bernardi M., da Costa L. N., Hoffman Y., Alonso M. V., Wegner G., Willmer C. N. A., Pellegrini P. S., 2001, *MNRAS*, 326, 375
 Zhao D. H., Mo H. J., Jing Y. P., Börner G., 2003, *MNRAS*, 339, 12

APPENDIX A: OTHER ADDITIONAL PARAMETER DISTRIBUTION SELECTION CRITERION

Rather than matching the mass distribution of the cluster-size random haloes to that of the Virgo haloes, it is possible to match other parameter distributions, namely to use another additional selection criterion besides the mass range. Each one of the subsamples obtained from the cluster-size random halo sample must reproduce one of the parameter distribution at redshift zero (X_0 , the only one that can be compared with the observational value measured for the Virgo cluster when possible) of the Virgo lookalike sample. The set parameter distribution of the random halo subsample is denoted X_0^s (always set at redshift zero).

Such an additional parameter selection criterion can give an idea of the commonness of the Virgo cluster with respect to that parameter within a group of its peers (cluster-size halo). Table A1 gives the number of random haloes left after applying successively

Table A1. Number of cluster-size random haloes available for comparisons with the 200 constrained haloes for each parameter distribution that is chosen to be set at redshift 0. Namely, we select only random haloes with a parameter, $X_{0,\text{rand}}$, such that it belongs to $[\bar{X}_{0,\text{virgo}} - 2 \times \sigma_{X_{0,\text{virgo}}}, \bar{X}_{0,\text{virgo}} + 2 \times \sigma_{X_{0,\text{virgo}}}]$, where $\sigma_{X_{0,\text{virgo}}}$ is the standard deviation of the $X_{0,\text{virgo}}$ and $\bar{X}_{0,\text{virgo}}$ is their mean at $z = 0$. In addition, random haloes in the tails of the distribution are only partially selected so that random and constrained distributions match each other.

Additional set parameter distribution at $z = 0$ (X_0^s)	Mass	Radius	Number of substructures	Velocity dispersion	Velocity	Centre of mass offset wrt to the spherical centre	Concentration	Spin
Random	77	82	75	101	66	259	374	359

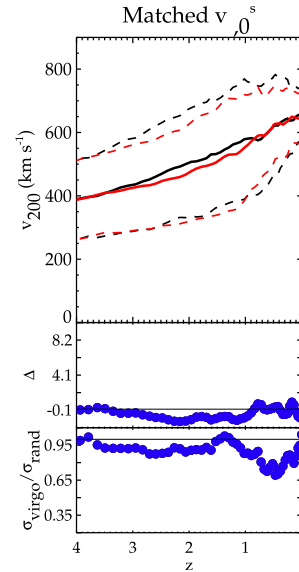


Figure A1. Same as Fig. 3, but cluster-size random haloes are selected so as to match their velocity distributions to those of the Virgo haloes.

the different X_0^s additional selection criterion. One can notice that clearly imposing the same velocity distribution to the random haloes as that of the Virgo haloes reduces drastically the number of cluster-size random haloes available for comparisons (66 random haloes out of 423 are left, i.e. 16 per cent). On the contrary, the NFW concentration has no serious effect (374 random haloes left, i.e. 88 per cent), while the centre of mass offset with respect to the spherical centre has only a mitigated impact (259 random haloes left, i.e. 61 per cent) on the number of random haloes left.

Note that, although in any case random haloes are selected to be within the same mass range as the Virgo haloes or in other words to have a cluster size, some subsamples are biased toward the low-mass (and all the other correlated parameters) end.

Fig. A1 shows the interesting case of the cluster-size random haloes selected according to their velocity value. At all redshifts the random and constrained mean velocities present no significant differences. Interestingly, the ratio of the constrained and random standard deviations is smaller than 1 for redshift higher than about 0.5 up to redshift 1. Note that once the velocity distribution is set to be the same at redshift zero for both the Virgo and cluster-size random haloes, they stay similar at higher redshifts. This highlights the large-scale correlation of the velocity field. It explains why the linear Reverse Zel'dovich Approximation used to put back constraints at the position of their precursors works well.

Tables A2 and A3 recapitulate the properties studied in the paper and highlight those atypical and/or constrained at redshift zero depending on the additional selection criterion (see the main core of the paper for details).

Table A2. Difference between the mean parameter values (Param., row) of the 200 Virgo haloes and of the selected random haloes. Cluster-size random haloes are selected according to the set parameter at redshift 0 (Param., column). A long dash (frame) stands for an (a highly) atypical property value (according to equation 1, absolute values above 3 and 9 in standard error units, respectively) for the Virgo haloes with respect to selected random haloes.

Param.	X_0^s : additional set parameter distribution at redshift 0							
	(1)	(2)	(3)	(4)	(5)	(6)	(7)	(8)
M_{200}	/							
R_{200}		/						
σ_v			/					
N_{substr}				/				
v					/			
CoM-off						/		
C_{NFW}							/	
Spin								/

Finally, Fig. A2 corresponds to one X_0^s case identified in the top right corner of the panel and by the largest symbol. The redshift of change stands up.

Table A3. Ratio of the standard deviations (Param., row) of the parameters of the 200 Virgo haloes and of the selected random haloes. Cluster-size random haloes are selected according to the set parameter at redshift 0 (Param., column). A long dash (frame) stands for a property that is (highly) constrained for the Virgo haloes with respect to the selected random haloes (values below 0.95 and 0.55, respectively).

Param.	X_0^s : additional set parameter distribution at redshift 0							
	(1)	(2)	(3)	(4)	(5)	(6)	(7)	(8)
M_{200}	/							
R_{200}		/						
σ_v			/					
N_{substr}				/				
v					/			
CoM-off						/		
C_{NFW}							/	
Spin								/

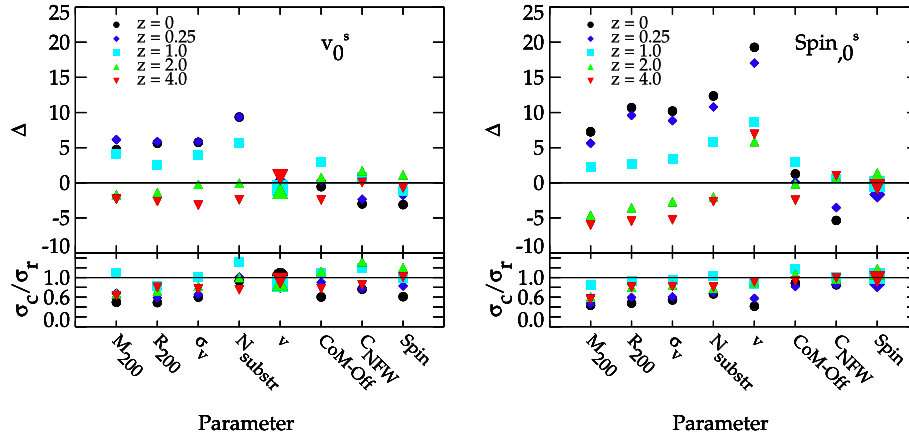


Figure A2. Each panel gives the quantitative measurement of the difference between the mean property values of the 200 Virgo haloes and of the cluster-size selected random haloes (top row, equation 1) as well as the ratio of their standard deviations (bottom row). Cluster-size random haloes are selected according to the set parameter (one by panel) at redshift 0 (name in the corner of each panel and largest symbol). Measurements are given at different redshifts (coloured symbols) in all the panels.

This paper has been typeset from a $\text{\TeX}/\text{\LaTeX}$ file prepared by the author.